THE INTERNATIONAL JOURNAL OF MEDICAL ROBOTICS AND COMPUTER ASSISTED SURGERY
Int J Med Robotics Comput Assist Surg 2010; **6**: 150–159.
Published online 23 March 2010 in Wiley InterScience (www.interscience.wiley.com). **DOI:** 10.1002/rcs.300

ORIGINAL ARTICLE

Human performance in the task of port placement for biosensor use#

Brady W. King[1]*
Luke A. Reisner[1]
R. Darin Ellis[2]
Michael D. Klein[3]
Gregory W. Auner[1]
Abhilash K. Pandya[1]

[1]*Department of Electrical and Computer Engineering, Wayne State University, Detroit, MI, USA*

[2]*Department of Industrial and Manufacturing Engineering, Wayne State University, Detroit, MI, USA*

[3]*Department of Pediatric Surgery, Children's Hospital of Michigan, and the Department of Surgery, Wayne State University School of Medicine, Detroit, MI, USA*

*Correspondence to: Brady W. King, 5050 Anthony Wayne Drive No. 3157, Detroit, MI 48202, USA.
E-mail: bwking@wayne.edu

#This work involved human subject testing that was approved by Wayne State University's Human Investigation Committee [HIC No. 082105B3E(R)]. The work did not involve animal testing or anything else that would raise ethical issues.

Accepted: 23 December 2009

Abstract

Background We conducted a study of participants' abilities to place a laparoscopic port for *in vivo* biosensor use. Biosensors have physical limitations that make port placement crucial to proper data collection. A new port placement algorithm enabled evaluation of port locations, using segmented patient data in a virtual environment.

Methods Port placement scoring algorithms were integrated into an image-guided surgery system. Virtual test scenes were created to evaluate various scenarios encountered during biosensor use. Participants were scored based on their ability to choose a port location from which points of interest could be scanned with a biosensor. Participants' scores were also compared to those of a port placement algorithm.

Results The port placement algorithm consistently outscored participants by 10–25%. Participants were inconsistent from trial to trial and from participant to participant.

Conclusion Port placement for biosensor procedures could be improved through training or augmentation. Copyright © 2010 John Wiley & Sons, Ltd.

Keywords port placement; sensor integration; image-guided surgery; Raman spectroscopy; medical robotics; virtual reality

Introduction

Biosensors are becoming more prevalent and more diverse in their capabilities. For example, some have the capability to diagnose disease *in vivo* and are now being designed for use in minimally invasive procedures. These biosensors are able to gather many types of data. For example, Raman spectroscopic probes are biosensors capable of distinguishing cancerous tissue from surrounding healthy tissue (1–4). This type of technology would allow surgeons to better decide which tissue to remove during a resection procedure (5–7).

Before a biosensor can be used in this fashion, a suitable port location must be chosen on the patient's skin. The port location is an opening through which the biosensor is threaded into the body. Because the port location is fixed, it affects where on the surface of the patient's tissue the biosensor can gather data. Many biosensors have physical constraints, such as a maximum angle of incidence or distance from the target surface. Outside of optimal conditions, the biosensor's ability to gather data is compromised. Therefore, the port location also determines the quality of data gathered from the patient's tissue.

In addition, many biosensors have a limited area from which data can be collected. For example, Raman spectroscopic probes typically gather data from an area $<150\ \mu m$ in diameter. This requires the sensor to be placed at many target points, compounding the problem of placement outside of optimal conditions. The port location must allow the biosensor to reach all areas of interest while preventing dangerous conditions, such as collisions with vital organs.

The limited view provided to the surgeons during a minimally invasive procedure, the complexity of tissue surfaces, the presence of obstructions and the physical limitations of biosensors make the task of port placement non-trivial. Some techniques have been created to automate this process (8–14). However, these techniques focus on the 'golden triangle' arrangement, which utilizes two ports for surgical manipulators and one port for a camera. This arrangement is used for current surgical procedures because it provides a comfortable working environment for the surgeon, with one hand on each side of the surgical site and a camera view in the centre. This arrangement, however, marginalizes a biosensor's ability to gather data because it does not account for the physical limitations in a biosensor's design.

For this reason, we have developed an automated port placement system that focuses on biosensors (15). The system utilizes 3D representations of a patient's anatomy derived from medical imaging (such as CT or MRI) and allows target areas to be selected by the surgeon. Along with these representations, the system uses several algorithms to test all potential port locations on the patient's skin. These algorithms ensure that the biosensor is long enough to reach target locations while meeting the positioning constraints of the biosensor. The algorithms also prevent collisions with other bodily structures. The system finds the best possible port location, which maximizes the ability of the biosensor to capture data from the specified target areas. In addition, the system has methods for evaluating (based on geometric and sensor constraints) the placement of a port chosen by a user. The implementation details of the system are presented in another paper (15).

In this paper, we investigate human performance in the task of port placement across a variety of scenarios. Using the automated port placement system's evaluation methods, we grade user-specified placement (15). Such an evaluation has never been done before because biosensor use has not been prevalent in surgery and no grading system was available for this type of port placement task. The information gathered from these tests will give us insight into human performance in the task of port placement for one class of biosensors (Raman). This should help in the development of training options to improve human performance. In addition, the results will help improve future automated systems to better augment human performance. We believe this will make the use of biosensors more feasible in the operating room.

Methods

Participants

This study was approved by the Human Investigation Committee at Wayne State University. Informed consent was obtained from each participant. A sample of 20 participants was chosen for testing, without exclusion criteria corresponding to adult age, gender or expertise. Fourteen participants were under the age of 30, four were women and two were surgeons. No participant had any previous training or experience with the tests being conducted, so their backgrounds had minimal influence on their performance.

Apparatus

Tests were performed on a laptop computer running 3D Slicer (16). This software application is a medical imaging package capable of displaying 3D representations of data, such as CT or MRI scans of patients. 3D Slicer was modified to incorporate the port placement algorithms described in (15). In addition, functions were added to collect data, such as the chosen port location during the testing. 3D test scenes were created, which consisted of individual 3D models representing different organs and bodily structures. The user interface consisted of a computer mouse that was used by the participants to choose a location in 3D space on the presented 3D scene.

Experimental task

Fifty tests were designed to mimic the requirements of biosensor port placement during surgery. They were developed with a specific biosensor in mind, a Raman spectrometer. This type of biosensor is capable of distinguishing between cancerous and non-cancerous tissue *in vivo* (17–19). This sensor was chosen because it is commercially available and is being used in ongoing research (20–22).

Each test scene consisted of 3D models representing the skin, target organs and the dimensions of a Raman probe (as a size reference). Rather than using complete scans of actual patients, the scenes were built from smaller sets of simpler 3D models. We did not use actual patient data because we did not want the subjects to be overly reliant on their medical knowledge. Moreover, actual patient data would be too geometrically complex and would not have given us control over specific dimensions of task difficulty.

Red markers were placed on the target organs to indicate points of interest that should be scanned with the Raman spectrometer (Figure 1). Across all 50 test scenes, there were a minimum of nine, a median of 54 and a maximum of 826 target points to scan from the selected port location.

The participants were instructed to pick a desired port location on the skin, using the mouse pointer. They were

DOI: 10.1002/rcs

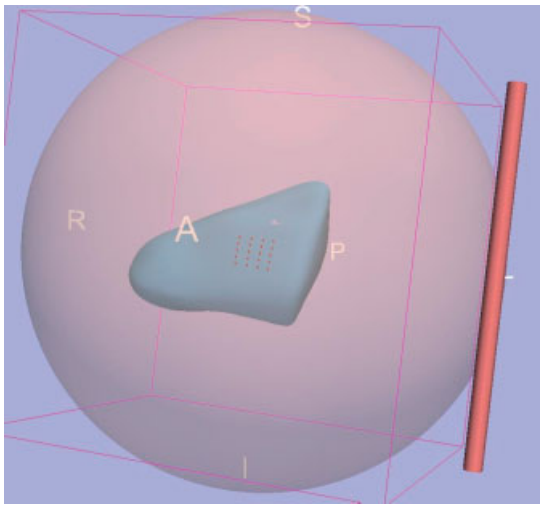

Figure 1. Example test scene from section 1. The pink sphere is the skin surface, and the enclosed blue model provides the target surface. The red dots represent target points. The red cylinder is a representation of the Raman probe, which provides a reference for scale. The letters are used by 3D Slicer to provide information about the current viewpoint (right, anterior, posterior, etc)

directed to choose a port location that would maximize the number of target points reachable with a virtual Raman probe. In addition, the participants were told about the limiting factors used by the port placement system to determine whether an individual target point is reachable. These factors are described below. The participants used the mouse to rotate, zoom and pan the virtual scene as desired, and they indicated their decision for the port location by pressing a button on a keyboard.

There are three factors evaluated by the port placement system to determine whether a target point is reachable. First, the ability of the virtual probe to reach the target point from the port location (via a straight line) is calculated. In other words, it is determined whether the probe has sufficient length. Second, a collision detection algorithm is executed to verify the absence of any obstructions between the target point and the port location, using the dimensions of the Raman probe. Finally, an algorithm calculates the angle of incidence of the biosensor from the target surface (at the target point) to determine whether the angle is within 45° of perpendicular. This constraint was chosen to imitate the characteristics of a real Raman probe, which can experience compromised data acquisition beyond this angle. If a target point passes all three tests, it is considered reachable.

Test scenes were created without regard to the number of target points that are actually reachable. Thus, participants did not know whether it was possible to reach every target point or only a subset of them. We used our automated port placement system to find an optimized port location for each test scene. As expected, the port placement system did not always reach 100% of the target points within the tolerance of the criteria for an allowable scan. Therefore, the number of points the port placement system reached was used to represent the maximum number of points reachable in each test scene.

Trial-level procedure

Each participant had to go through all 50 test scenes. The tests were presented in random order, with one test shown at a time. Once a participant chose a port location, the next test was presented immediately. No feedback was given to the participant as to the quality of his performance. This was done to minimize learning effects throughout the study. The execution of one test by a participant was considered to be one trial.

Experimental design

The 50 tests were divided into five sections, with 10 tests in each section. Each section was designed to test a specific condition related to the task of port placement. These specific conditions were decided upon during a discussion with a surgeon. The surgeon was asked what types of conditions would present difficulties when trying to laparoscopically position a biosensor to scan target tissues. The surgeon indicated four conditions in which biosensor sampling would be impeded due to improper port placement. Four sections of the study were derived from these problem conditions. A fifth section with no significant impediments was added as a control case. These test sections are described in greater detail below.

The first section of 10 tests served as a baseline/control condition; it was designed to be simple. In this type of scenario, the skin surface and target surfaces were smooth or flat, and the line from the ideal port location to the target surface was roughly orthogonal to the target surface. The number of target points was small and they were clustered close together. Figure 1 shows an example from this section.

The second section of tests focused on complex target surfaces. In this type of scenario, the skin surface was smooth, but the target surfaces were bumpy or contained complex angles and grooves. The target points remained relatively few in number and clustered close together. Figure 2 shows an example from this section.

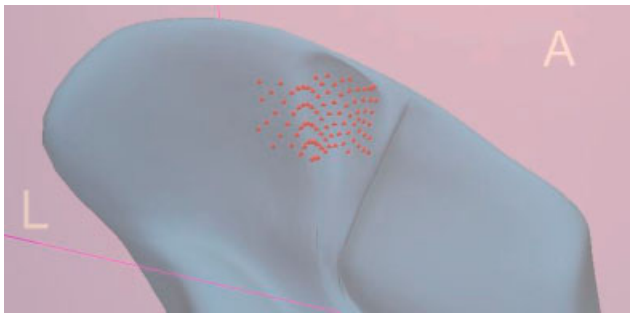

Figure 2. Close-up view of a section 2 test scene that demonstrates a complex target surface

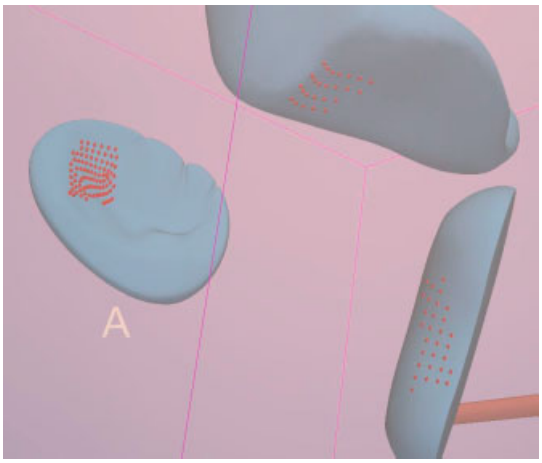

Figure 3. Close-up view of a section 3 test scene that demonstrates large target surface area

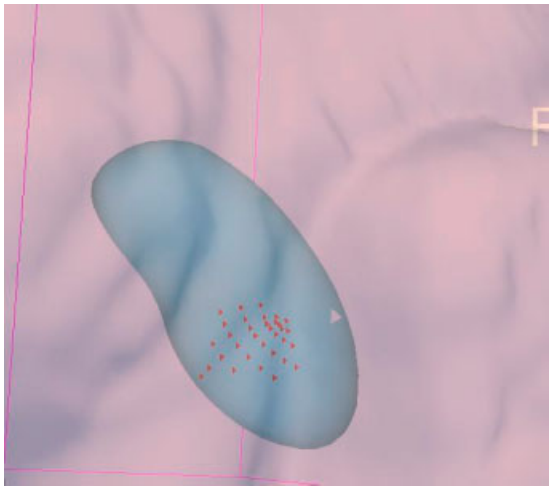

Figure 4. Close-up view of a section 4 test scene that demonstrates a complex skin surface

The third section of tests focused on the size of the target surface. In this type of scenario, the skin surface and target surfaces were smooth. The number of target points was large and there were some cases in which groups of target points were separated by distance from each other. Figure 3 shows an example from this section.

The fourth section of tests focused on the complexity of the skin surface. In this type of scenario, target surfaces were smooth, but the skin surface was bumpy or contained complex angles and grooves. The number of target points was relatively small and they were clustered close together. Figure 4 shows an example from this section.

The final section of tests focused on obstructions. In this section, the skin surface and target surfaces were smooth. The number of target points was small and they were clustered close together. However, additional surfaces were placed in positions that would obstruct the placement of the port. Figure 5 shows an example from this section.

Each participant was presented with each test once. The trials were analysed independently, and the performances

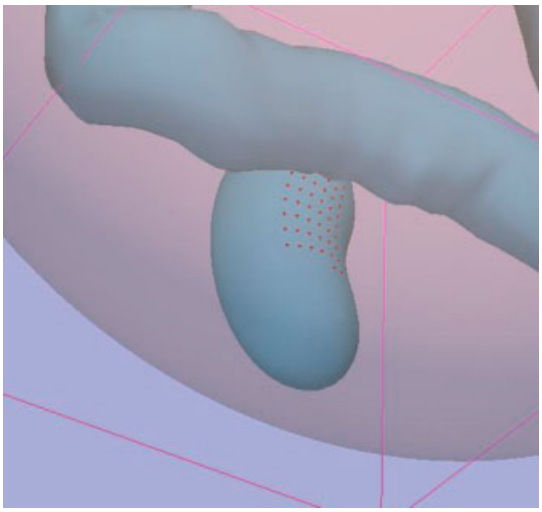

Figure 5. Close-up view of a section 5 test scene that demonstrates an obstruction

of different participants served as replicates of the experiment for statistical analysis. The time for each test was not considered. The only data collected during testing were the Cartesian coordinates (x, y, z) of the port location chosen by the participant for each test.

Although there were no time constraints placed upon the subjects during the testing, the tests were designed to be completed in about 30–45 min. Since only a mouse and keyboard had to be used during the tests, no physical exertion was required. Since there were no time constraints or performance requirements, little mental stress was placed upon the participants. Consequently, fatigue was not found to be an issue during the testing.

Post-processing was done using the port placement system's evaluation methods. Participants were given a score for each test that was equal to the number of target points reachable with the virtual Raman probe from the participant's chosen port location. An individual target point was considered reachable if the three criteria described in the 'Experimental task' section were met.

From the score (the number of reachable target points) that each participant achieved for each test scene, two percentages were calculated. The first was the participant's score divided by the maximum number of reachable target points, or the percentage of maximum (PoM). As stated before, the maximum number of reachable target points was determined using the port placement system. The second was the participant's score divided by the total number of target points present in the scene, or the percentage of total (PoT).

It was important to obtain a measure of the difficulty of each of the five test sections. To calculate this, we obtained the average of the PoMs for all participants in all tests of each test section. PoM was used because it utilized the port placement system's score as the maximum number of points. This normalized the results among scenes that had different amounts of reachable target points.

DOI: 10.1002/rcs

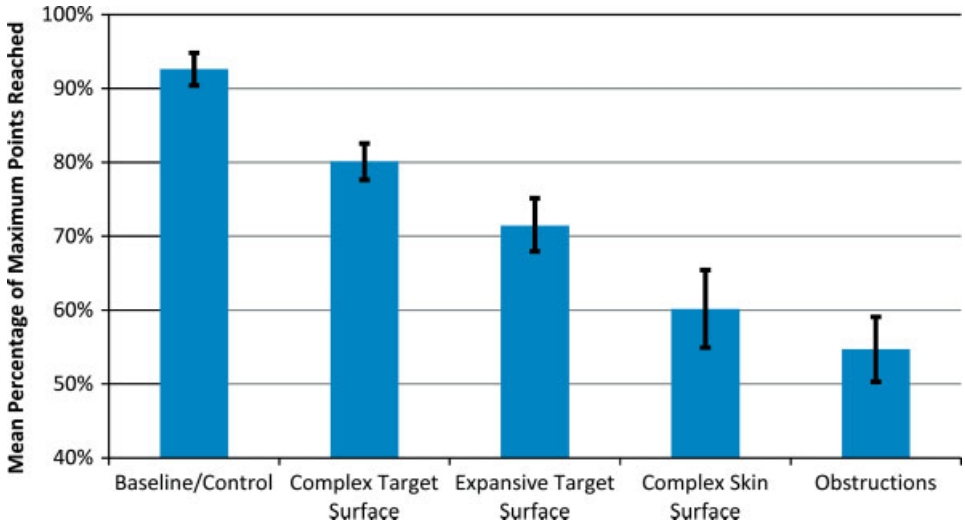

Figure 6. Average percentage of maximum (PoM) points reached for each test section. The black vertical lines represent the 95% confidence interval about each mean

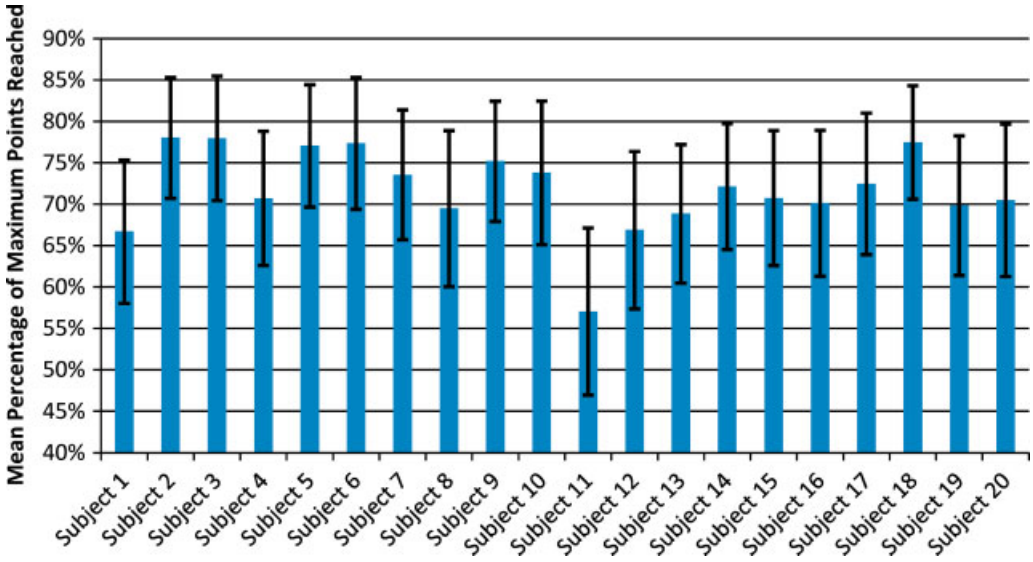

Figure 7. Average percentage of maximum (PoM) points reached for each participant over all test scenes. The black vertical lines represent the 95% confidence interval about each mean

Results

We used the average of the PoMs to compare the different scenarios to each other, based on difficulty, in order to provide an indication of the types of scenarios in which human performance suffers. Figure 6 shows the averages obtained and the 95% confidence interval for each test section.

The participants' average PoMs across all scenes were in the range 57–78%. Confidence intervals of the mean PoMs were calculated for all participants, and inspection of the interval plots did not reveal any outlying participants. Figure 7 shows the average PoM and 95% confidence interval for each participant.

In addition, it was also important to investigate performance on a scene-by-scene basis. This provided an opportunity to find scenes in which the difference between the average participant performance and the computer algorithm's performance was greater than other scenes in the same test section. These outlying scenes can help us understand specific scenarios in which performance is degraded. To calculate this, we obtained the average of the PoTs for all participants for each scene. PoT was used in this case to better compare the performances of the port placement system and the participants. The following graphs display the results of the calculations, with one graph per test section. For clarity, the graphs' contents are sorted by ascending computer algorithm performance.

The baseline/control section represented the first type of scene. As shown in Figure 8, average participant performance was in the range 0–19% less than the computer's results. This was expected because these tests were the easiest.

DOI: 10.1002/rcs

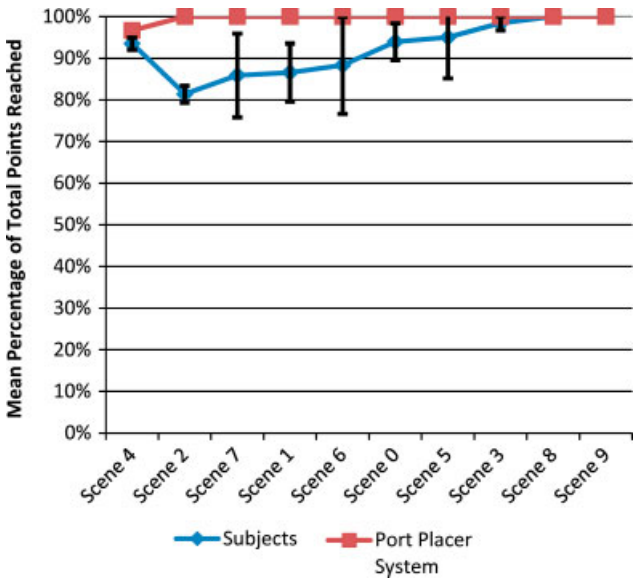

Figure 8. Performance for the baseline/control section. Squares represent the port placer system's performance, while diamonds represent the average participant performance. The black vertical lines represent the 95% confidence interval about each mean

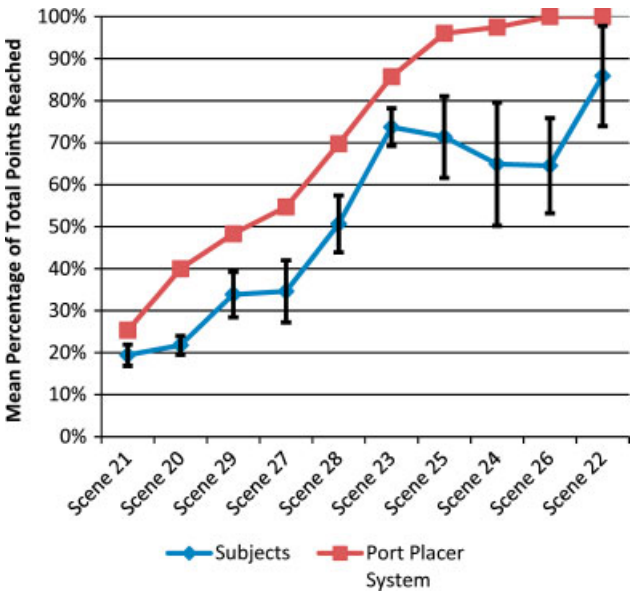

Figure 10. Performance for the expansive target surface section. Squares represent the port placer system's performance, while diamonds represent the average participant performance. The black vertical lines represent the 95% confidence interval about each mean

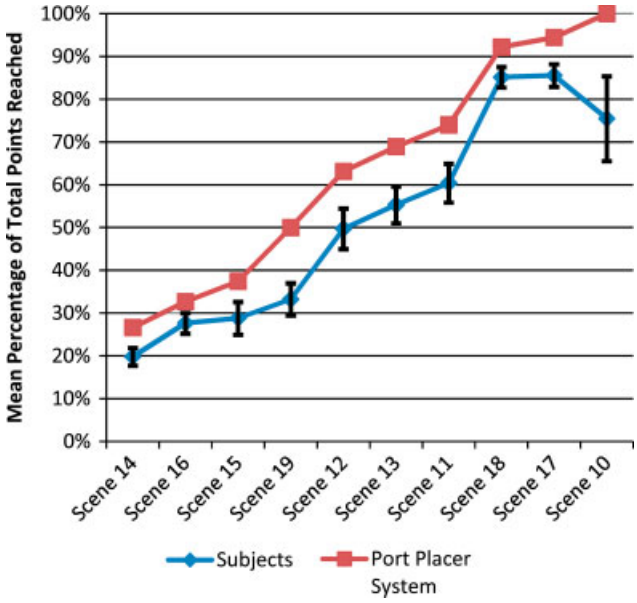

Figure 9. Performance for the complex target surface section. Squares represent the port placer system's performance, while diamonds represent the average participant performance. The black vertical lines represent the 95% confidence interval about each mean

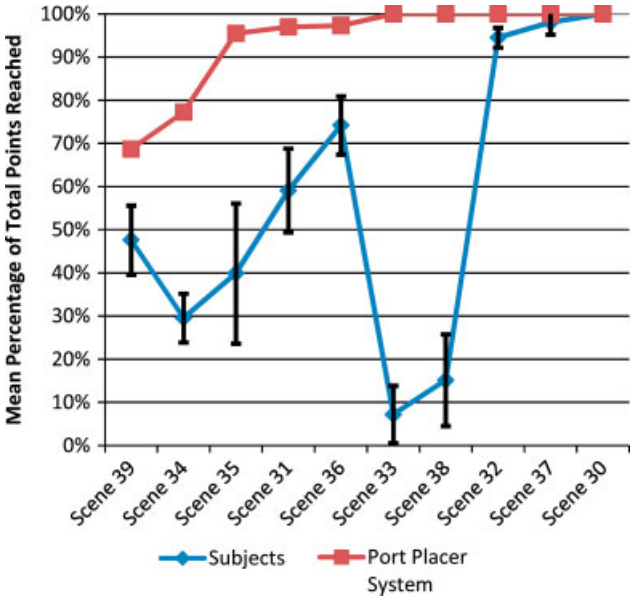

Figure 11. Performance for the complex skin surface section. Squares represent the port placer system's performance, while diamonds represent the average participant performance. The black vertical lines represent the 95% confidence interval about each mean

The complex target surface section represented the second type of scene. As shown in Figure 9, average participant performance was in the range 6–25% less than the port placement system's results.

The expansive target surface section represented the third type of scene. As shown in Figure 10, average participant performance was in the range 6–35% less than the computer's results.

The complex skin surface section represented the fourth type of scene. As shown in Figure 11, average participant performance was in the range 0–93% less than the port placement system's results.

The obstructions section represented the fifth type of scene. As shown in Figure 12, average participant performance was in the range 5–43% less than the computer's results.

DOI: 10.1002/rcs

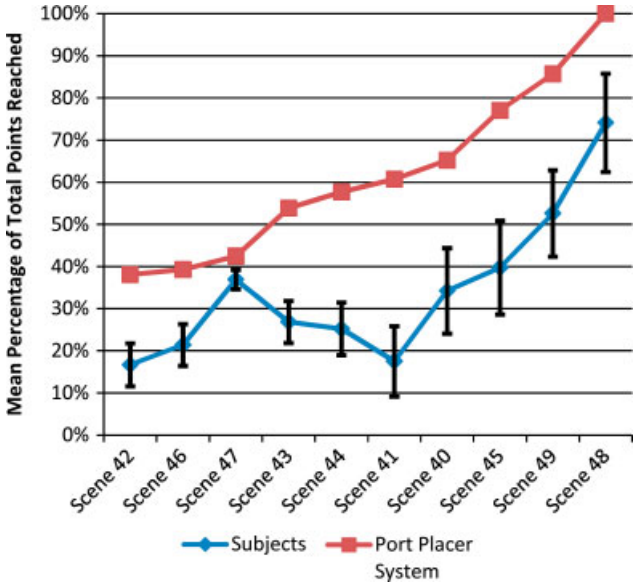

Figure 12. Performance for the obstructions section. Squares represent the port placer system's performance, while diamonds represent the average participant performance. The black vertical lines represent the 95% confidence interval about each mean

Discussion

The results demonstrate that human performance tends to lag behind the port placement system's performance by 10–25% (on average). However, there were many cases where human performance was significantly lower than the ideal performance of the port placement system. This section aims to identify conditions that led to these drops in performance.

Separating ridge

Scene 10 (from the complex target surface section) demonstrated a target surface with target points on both sides of a ridge. In this case, the participants' tendency was to assume that not all of the points could be reached. Therefore, they chose to concentrate on obtaining a better score on just one side of the ridge. The computer system demonstrated that it is indeed possible to reach 100% of the points in this test. Figure 13 shows an example of this scenario.

Multiple targets separated by distance

Scenes 24, 25 and 26 (from the expansive target surface section) demonstrated multiple groups of target points separated by distance. This case was an extension of the previous case (separating ridge). As in the previous section, the participants had a tendency to focus on reaching one group of points with high accuracy, rather than trying to reach both groups with less accuracy. As before, the computer system showed that is preferable to

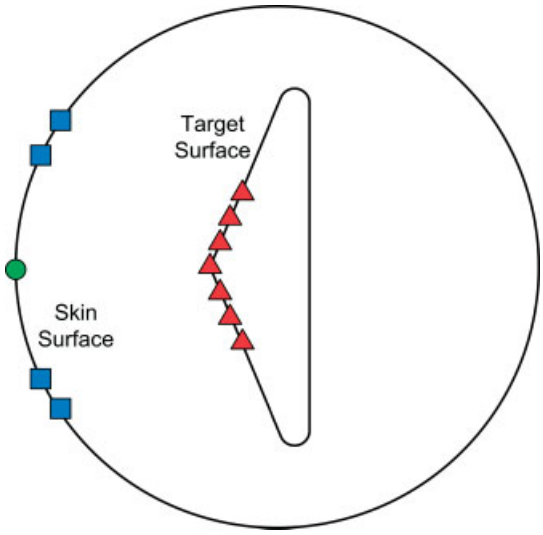

Figure 13. Example of the 'separating ridge' scenario. The green circle represents the correct choice for port placement, while the blue squares represent typical choices made by participants. The red triangles represent the target points

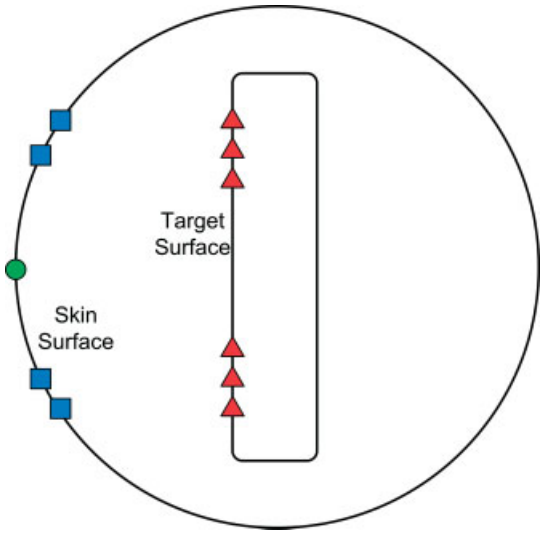

Figure 14. Example of the 'multiple targets separated by distance' scenario. The green circle represents the correct choice for port placement, while the blue squares represent typical choices made by participants. The red triangles represent the target points

reach for both groups of points. Figure 14 provides an example of this scenario.

Significant distance from target

Exceptionally low performance was observed for scenes 33, 35 and 38 (from the complex skin surface section). Upon review, it was discovered that these trials contained a second element of difficulty beyond the complex skin surface. The potential port locations that the target surface directly faced (the port locations that would otherwise provide the highest score) were too far away from the skin surface for the probe to reach. Some participants

chose these locations regardless, whereas others chose port locations along the side. The extra variable of distance (in addition to the angle of incidence at the target surface) resulted in participants choosing widely varying port locations. Figure 15 provides an example of these results.

Indented ridge

Scenes 31 and 34 (from the complex skin surface section) had target surfaces very near the skin surface, as well as ridges in the skin surface near the optimal port location.

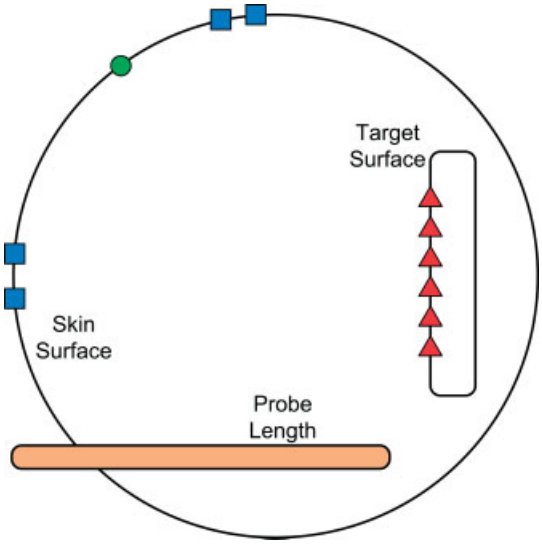

Figure 15. Example of the 'significant distance from target' scenario. The green circle represents the correct choice for port placement, while the blue squares represent typical choices made by participants. The red triangles represent the target points. The probe model was shown in all scenes to give participants a representation of its length

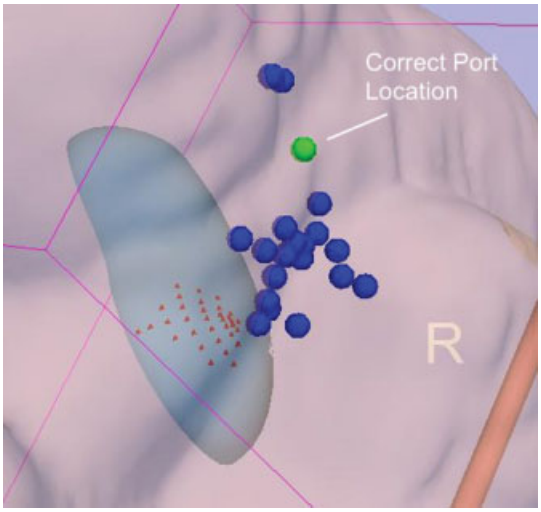

Figure 16. Example of the 'indented ridge' scenario. The correct choice for port placement (the green circle) is surrounded by the choices of participants (blue circles). The red triangles represent the target points

As shown in Figure 16, it appears that participants were picking port locations along a ridge. This may have been because the ridge was indented and picking points within this indent would serve to minimize the distance to the target surface. However, the distance to the target surface was not an issue in these scenes (unlike the scenes mentioned in the previous section). The challenge of the complex skin surface may have led participants to focus on what seemed to be a simple solution (minimizing the distance), even though it did not provide an optimal placement. Figure 16 shows the results of scene 34.

Obstructions

Highly inconsistent levels of performance were observed for the obstructions section. Some scenes resulted in relatively good performance, whereas others produced very poor results. Looking closely at the geometric distributions of chosen port locations, there is clearly better performance for scenes in which the obstruction was positioned in a manner that obviously limited the choice to one area on the skin surface. The scenes with worse performance had obstructions that made the choice less obvious. In these cases, the placement of the port varied significantly, leading to poor average performance. Figure 17 shows both cases.

Conclusion

Proper port placement is critical to a biosensor's ability to gather high-quality data and to a surgeon's ability to perform a successful biopsy. Thus, it is important to evaluate the ability of people to find optimal port locations. An optimized port placement system was developed to select the best port location, based on the surgeon's area of interest, the biosensor's characteristics and the patient's anatomy. This system was used to analyse the port selection performance of a group of participants over a variety of test scenarios. The scenarios were designed to investigate different challenges involved in the selection of a port location.

A number of conclusions can be drawn from the analysis of the participants' performance. The first is that the participants uniformly obtained scores approximately 10–25% below the scores obtained by the port placement system. This was expected, due to the algorithm's exhaustive search technique for obtaining port locations. However, this indicates that human performance could be improved, perhaps through better training.

From Figures 8–12, we see that the 95% confidence interval of the percentage of target points reached in a given scene was generally 10–20% about the mean. Thus, the number of points reached in a scene was relatively inconsistent. Because the number of reachable points is directly related the quality of the chosen port location, we can infer that the test participants picked port locations of

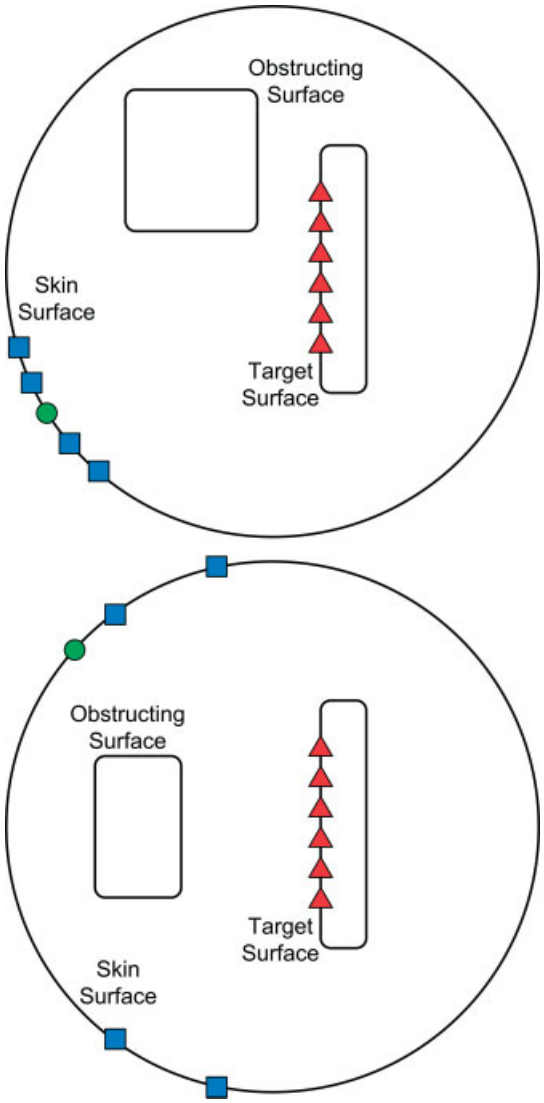

Figure 17. Examples of the 'obstructions' scenario. The top diagram demonstrates a scenario in which the choice is obvious, whereas the bottom demonstrates a scenario in which the choice is ambiguous. The green circles represent the correct choices for port placement, while the blue squares represent typical choices made by participants. The red triangles represent the target points

varied quality. Therefore, the second conclusion we can make is that the quality of port locations chosen for a given scene was inconsistent among participants.

In addition, Figure 7 shows that, for each participant, the 95% confidence interval across all scenes was generally 15%. Consequently, the third conclusion is that the number of reachable points (and thus the port location quality) a given participant achieved was inconsistent from scene to scene.

Lastly, we can see that no one participant vastly outperformed the other participants over the entire experiment. This information allows us to conclude that participants had similar performance on average over the entire test space, despite the fact that port placement was generally inconsistent from participant to participant for any given test scene.

The results of this study suggest some ways to improve human performance. It may be possible to use the port placement system and the data gathered here to create a training programme. Since feedback was not provided to participants during the tests, a minimal amount of learning was able to occur during the tests. By adding modifications to collect and present different performance metrics, it is envisioned that the system could be used as a training tool. For example, by focusing on the areas where performance was degraded and using the computer system to indicate proper placement, it may be possible to increase human performance. In addition, further collection and analysis of data may indicate ways to make the port selection process easier for people.

We identified a common source of error in the Discussion section for tests involving a significant distance from the target. Subjects erroneously chose port locations that were too distant from the target for the probe to reach the surface. A potential way to improve performance would be to add a virtual tool or measurement device that could be positioned at a chosen port location to evaluate the ability of the probe to reach the target surface. The effects of such a tool could be analysed as part of a future study.

With enhancements and further testing of the port placement system, varying levels of human augmentation and even automation may be possible. Using preoperative patient imaging, the system could be used to select port locations with minimal human intervention. To assist surgeons in physically creating a port in a patient at the determined location, an augmented reality interface with positioning cues could be implemented (23). Furthermore, if the system were integrated with a medical robot, the selected port location could be reached automatically.

Surgeon feedback may suggest further improvements that can be made to the port placement system. One possible improvement would be allowing multiple port locations to be determined. This would enable the system to reach more target points (if the surgeon deemed multiple ports to be acceptable). In addition, it would enable the system to be generalized for use in laparoscopic and robotic cases (where multiple ports are required). Another related potential improvement would be generalizing the port placement algorithms to work with tools other than biosensors. Together, these improvements could have broader impacts in port placement during neurosurgery and laparoscopic procedures.

For the next step in this work, we plan to implement the training tool described above. We will then conduct further subject testing to determine whether the system provides any measurable benefit in human performance. To make the port placement system more practical, we plan to investigate the incorporation of real-time imaging techniques (24,25). Real-time imaging could be used to enable the system to handle tissue movements due to respiration, insufflation, organ shift, etc. Since real-time imaging is an active area of research, we will continue to monitor the state of the art to look for feasible

implementations. Lastly, we plan to add support for other types of biosensors to the system.

In summary, we have identified scenarios in which human performance is degraded in the task of port placement for biosensor use. Because of the importance of a port's placement to the operation of a biosensor, this study suggests improving performance through the use of automated port placement or focused training programmes.

Acknowledgements

This work was supported in part by the Endowment for Surgical Research (ENSURE) at Children's Hospital of Michigan.

References

1. Rabah R, Weber R, Serhatkulu GK, *et al*. Diagnosis of neuroblastoma and ganglioneuroma using Raman spectroscopy. *J Pediat Surg* 2008; **43**(1): 171–176.
2. Haka AS, Shafer-Peltier KE, Fitzmaurice M, *et al*. Identifying microcalcifications in benign and malignant breast lesions by probing differences in their chemical composition using Raman spectroscopy. *Cancer Res* 2002; **62**(18): 5375–5380.
3. Haka AS, Shafer-Peltier KE, Fitzmaurice M, *et al*. Diagnosing breast cancer by using Raman spectroscopy. *Proc Natl Acad Sci USA* 2005; **102**(35): 12371–12376.
4. Lorincz A, Haddad D, Naik R, *et al*. Raman spectroscopy for neoplastic tissue differentiation: a pilot study. *J Pediat Surg* 2004; **39**(6): 953–956.
5. Reisner LA, King BW, Klein MD, *et al*. A prototype biosensor-integrated image-guided surgery system. *Int J Med Robotics Comput Assist Surg* 2007; **3**(1): 82–88.
6. Wills H, King B, Reisner L, *et al*. Robotically positioned Raman spectroscopy probe for cancer resection. SAGES Meeting, Philadelphia, PA, 9–12 April 2008; 328–329.
7. King BW, Reisner LA, Klein MD, *et al*. Registered, sensor-integrated virtual reality for surgical applications. IEEE Virtual Reality Conference, Charlotte, NC, 10–14 March 2007; 277–278.
8. Cannon JW, Stoll JA, Selha SD, *et al*. Port placement planning in robot-assisted coronary artery bypass. *IEEE Trans Robotics Autom* 2003; **19**(5): 912–917.
9. Chiu AM, Dey D, Drangova M, *et al*. 3D image guidance for minimally invasive robotic coronary artery bypass. *Heart Surg Forum* 2000; **3**(3): 224–231.
10. Selha S, Dupont P, Howe R, *et al*. Dexterity optimization by port placement in robot-assisted minimally invasive surgery. In *Telemanipulator and Telepresence Technologies VIII; 28 October 200*, Stein MR (ed.). SPIE: Newton, MA, 2002; 97–104.
11. Tabaie HA, Reinbolt JA, Graper WP, *et al*. Endoscopic coronary artery bypass graft (ECABG) procedure with robotic assistance. *Heart Surg Forum* 1999; **2**(4): 310–317.
12. Trejos AL, Patel RV, Ross I, *et al*. Optimizing port placement for robot-assisted minimally invasive cardiac surgery. *Int J Med Robotics Comput Assist Surg* 2007; **3**(4): 355–364.
13. Navab N, Traub J, Sielhorst T, *et al*. Action- and workflow-driven augmented reality for computer-aided medical procedures. *IEEE Comput Graphics Appl* 2007; **27**(5): 10–14.
14. Traub J, Feuerstein M, Bauer M, *et al*. Augmented reality for port placement and navigation in robotically assisted minimally invasive cardiovascular surgery. In *Computer Assisted Radiology and Surgery, Chicago, IL, 23–26 June 2004*, Lemke HU, Inamura K, Doi K, *et al*. (eds). Elsevier: New York, 2004; 735–740.
15. King BW, Reisner LA, Ellis RD, *et al*. Optimized port placement for *in vivo* biosensors. *Int J Med Robotics Comput Assist Surg* 2009; **5**(3): 267–275.
16. Gering DT, Nabavi A, Kikinis R, *et al*. An integrated visualization system for surgical planning and guidance using image fusion and an open MR. *J Magnet Reson Imaging* 2001; **13**(6): 967–975.
17. Motz JT, Gandhi SJ, Scepanovic OR, *et al*. Real-time Raman system for *in vivo* disease diagnosis. *J Biomed Optics* 2005; **10**(3): 031113.
18. Haka AS, Volynskaya Z, Gardecki JA, *et al*. *In vivo* margin assessment during partial mastectomy breast surgery using Raman spectroscopy. *Cancer Res* 2006; **66**(6): 3317–3322.
19. Bakker Schut TC, Witjes MJH, Sterenborg HJCM, *et al*. *In vivo* detection of dysplastic tissue by raman spectroscopy. *Anal Chem* 2000; **72**(24): 6010–6018.
20. Matousek P, Stone N. Emerging concepts in deep Raman spectroscopy of biological tissue. *Analyst* 2009; **134**(6): 1058–1066.
21. Wills H, Kast R, Stewart C, *et al*. Diagnosis of Wilms' tumor using near-infrared Raman spectroscopy. *J Pediat Surg* 2009; **44**(6): 1152–1158.
22. Nijssen A, Koljenovi S, Schut TCB, *et al*. Towards oncological application of Raman spectroscopy. *J Biophoton* 2009; **2**(1–2): 29–36.
23. King BW, Reisner LA, Dworzecki ST, *et al*. Fusion of tomographic imaging with *in vivo* Raman cancer diagnosis using augmented reality. *Computer Assisted Radiology and Surgery, Barcelona, Spain, 25–28 June 2008*. Springer: Berlin, 2008; S274.
24. Chrisochoides N, Fedorov A, Kot A, *et al*. Toward real-time image-guided neurosurgery using distributed and grid computing. *ACM/IEEE Conference on Supercomputing, Tampa, Florida, 11–17 November 2006*. ACM: New York, 2006.
25. Meier U, López O, Monserrat C, *et al*. Real-time deformable models for surgery simulation: a survey. *Comput Methods Programs Biomed* 2005; **77**(3): 183–197.